Optics Letters

Ultra-compact silicon mode (de)multiplexer based on directional couplers with subwavelength sidewall corrugations

Xiaofei Wang,[1] Hui Yu,[1,2,*] Qiang Zhang,[2] Zhilei Fu,[1] Penghui Xia,[1] Qikai Huang,[1] Nannan Ning,[1] Zhujun Wei,[1] Yuehai Wang,[1] Xiaoqing Jiang,[1] and Jianyi Yang[1]

[1]Institute of Integrated Microelectronic Systems, College of Information Science and Electronic Engineering, Zhejiang University, Hangzhou 310027, China
[2]Zhejiang Lab, Hangzhou 311121, China
*Corresponding author: huiyu@zju.edu.cn

Received 24 November 2021; revised 20 February 2022; accepted 22 February 2022; posted 23 February 2022; published 19 April 2022

Asymmetrical directional couplers aided with subwavelength sidewall corrugations are used to realize ultra-compact silicon mode (de)multiplexers at C-band. Three mode (de)multiplexers with ultra-short coupling lengths of 5.6/6.5/7.7 μm are designed to enable low-loss mode conversions between TE_0 and $TE_{1/2/3}$ modes. They are then cascaded to build a four-channel mode-division-multiplexing (MDM) link. The four mode channels present minimal on-chip insertion losses of 0.2/0.7/0.7/0.9 dB at their peak wavelengths. Measured cross talk levels of the four mode channels are better than −18.0/−19.1/−16.0/−18.2 dB within the wavelength range from 1530 nm to 1580 nm.

https://doi.org/10.1364/OL.449493

Due to the explosive increase in the number of mobile terminals and the rapid development of cloud computing services, the demand on the transmission bandwidth of optical communication systems has grown exponentially [1–3]. Multiple multiplexing technologies by exploiting different degrees of freedom of light have been developed to enhance the transmission capacity of the fiber [4–7]. Among them, the wavelength division-multiplexing (WDM) technology is the most successful and thus has already been widely used in practical systems. It is known that the total channel number of a WDM system is usually constrained by the cost and complexity. After the developments in these next few years, the capacity of the WDM technology is going to reach a bottleneck [8,9]. Therefore, other multiplexing technologies such as the mode division multiplexing (MDM) [10–12] are projected to play important roles in future.

The MDM technology employs orthogonal guiding modes in a multimode bus waveguide to carry different data streams, and hence is beneficial to reduce the number of laser diodes (LD). An essential element in the MDM network is the mode (de)multiplexer which converts fundamental modes in different adding ports to corresponding high-order modes in the bus waveguide or vice versa. Reported mode (de)multiplexers are usually based on structures such as multimode interference (MMI) couplers [10,12], asymmetric Y-junctions [11,13], asymmetric directional couplers (DCs) [9,14], and adiabatic DCs [15]. The MMI-based mode (de)multiplexers are subjected to a very limited mode channel number, while those based on asymmetric Y-junctions demand sharp tips which are hard to pattern. In contrast, the (de)multiplexers based on asymmetric DCs or adiabatic DCs have relatively larger minimum feature sizes. Furthermore, their channel count can be increased easily by cascading more DCs. Despite these advantages, typical lengths of the DCs on silicon range from several tens to several hundreds of micrometers. The footprint thus emerges as a limiting factor of the total channel count. To address this issue, inverse design methods such as the topology optimization [16] and the nonlinear direct-binary-search optimization algorithms [17] are used to miniaturize silicon mode (de)multiplexers. Devices with footprints as small as a few micrometers are successfully demonstrated. However, to design high-order mode demultiplexers with the inverse design method is not straightforward. Therefore, corresponding devices usually present higher insertion losses and fewer mode numbers.

In this Letter, we demonstrate an ultra-compact silicon mode (de)multiplexer by using asymmetric directional couplers with subwavelength grating (ADCSWG) [18]. The sub-wavelength structures weaken the mode confinement in the lateral direction. Ultimately, the interaction between the two coupled modes is greatly enhanced to shorten the coupling length. Compared with previous works, this scheme simultaneously possesses merits of low insertion loss, compact footprint, relaxed requirement on the fabrication resolution, and moreover, its channel count can be increased easily.

A schematic diagram of the four-channel mode multiplexer is shown in Fig. 1. Incident fundamental modes from the three adding ports are coupled to the first three high-order modes in the bus waveguide by three serially cascaded ADCSWGs. As shown in Fig. 1(b), each ADCSWG consists of a single-mode access waveguide and a multimode bus waveguide. Their widths are tailored carefully to satisfy the phase matching condition of the two mutually coupled modes [9]. Inside the coupling gap, both waveguides incorporate subwavelength sidewall corrugations

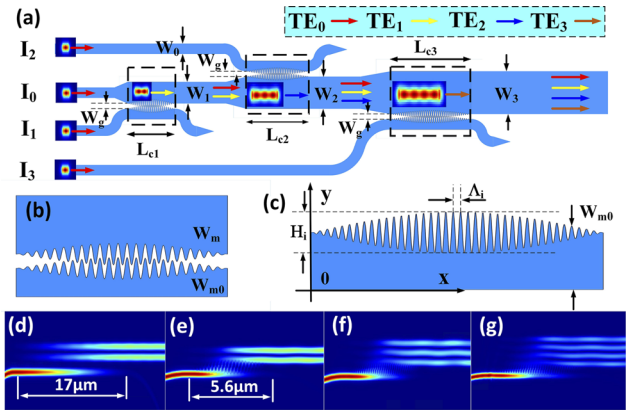

Fig. 1. Schematic diagrams of (a) the 1×4 mode (de)multiplexer based on the ADCSWGs, (b) the coupling gap, and (c) the subwavelength sidewall corrugation. Simulated optical field distributions of mode conversions from TE_0 to high-order modes in (d) conventional ADC and (e)–(g) ADCSWGs at 1.55 μm.

which interlace with each other. To suppress the backreflection of light, the corrugation depth varies gradually along the beam propagation direction. An optimized shape function of the sinusoidal corrugation is written as [18]

$$W_{m0}(x) = W_{m0}(0) - H_m/2 \times \sin(\pi x/L_{cm}) \sin(2\pi x/\Lambda_m), \quad (1)$$

$$W_m(x) = W_m(0) + H_m/2 \times \sin(\pi x/L_{cm}) \sin(2\pi x/\Lambda_m), \quad (2)$$

where $W_{m0}(x)$ and $W_m(x)$ are the widths of the access waveguide and the bus waveguide at the position x; $W_{m0}(0)$ and $W_m(0)$ denote the widths of the access waveguide and the bus waveguide at the initial part ($x = 0$) of the ADCSWG; H_m and Λ_m denote the maximum depth and the pitch of the corrugation, respectively; and L_{cm} is the coupling length. The subscript m represents the converted mode order. Definitions of these parameters have been marked in Fig. 1(c). Compared with saw-teeth and comb-teeth, the sinusoidal corrugation is less sensitive to quantization errors caused by the limited lithography grid size [19] and the reactive ion etching (RIE) lag effect [20], so it is much easier to pattern.

According to the effective medium theory, the coupling gap with subwavelength sidewall corrugations can be regarded as an homogeneous medium with a raised effective refractive index of n_e [21]. Owing to the reduced refractive index contrast between waveguide cores and the gap region, optical field confinements of the two coupled waveguides are weakened to enhance their coupling strength. As a result, the coupling length could be greatly shortened.

The width of single-mode access waveguides is chosen to be $W_{m0}(0) = 0.4$ μm, and the gap at the initial part of the ADCSWG is $W_g = 0.2$ μm. The bus waveguide uses different widths at the three ADCSWG sections to meet the corresponding phase matching conditions. Adiabatic tapers connect different segments of the bus waveguide. We employ the finite difference eigenmode (FDE) solver (Lumerical MODE Solutions) to numerically calculate effective indices of involved modes at different waveguide widths. On basis of the simulation result, the widths of the bus waveguide are chosen to be $W_{1/2/3}(0) = 0.82/1.232/1.66$ μm for mode conversions from TE_0 to $TE_{1/2/3}$.

Coupling lengths, corrugation heights, and pitches of the three ADCSWGs should be optimized to maximize their mode

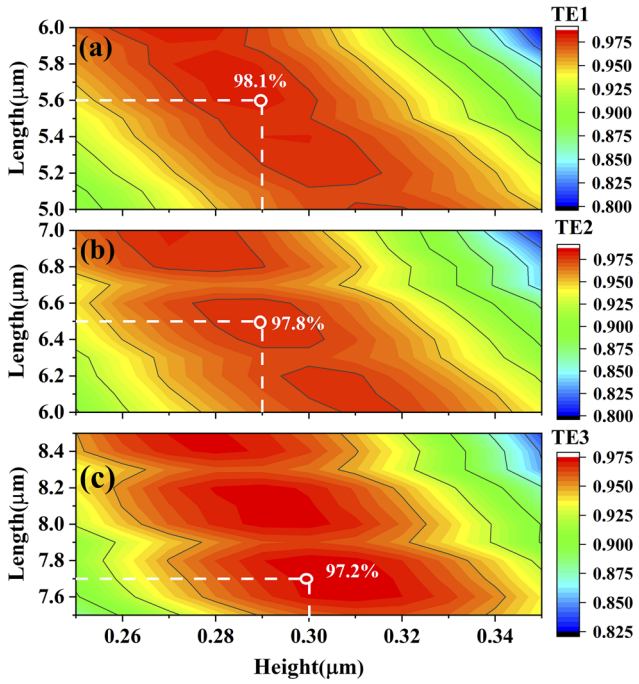

Fig. 2. Simulated contour maps of coupling efficiencies as functions of corrugation heights and coupling lengths at 1.55 μm for (a) TE_0 to TE_1, (b) TE_0 to TE_2, and (c) TE_0 to TE_3 mode conversions.

conversion efficiencies. At first, the three ADCSWGs use a uniform corrugation pitch of $\Lambda_m = 0.2$ μm. Under this condition, the effective index of the Bloch–Floquet mode is below the Bragg threshold, and the three ADCSWGs operate in the deep-subwavelength regime [21]. After that, corrugation heights and coupling lengths are determined through numerical simulation. Simulated coupling efficiencies as functions of corrugation heights and coupling lengths are plotted in Fig. 2 for the three ADCSWGs at 1550 nm. These contour maps indicate that if one wants to shorten the coupling length, the corrugation height should be raised accordingly so as to avoid the degradation of coupling efficiency. However, increasing the corrugation height would reduce the space between two interlaced sidewall corrugations. Therefore, in view of the minimal feature size, corrugation heights and coupling lengths of the three ADCSWGs are chosen to be $H_{1/2/3} = 0.29/0.29/0.3$ μm and $L_{c1/2/3} = 5.6/6.5/7.7$ μm, respectively. The resultant mode conversion efficiencies between TE_0 mode and $TE_{1/2/3}$ modes are 98.1%/97.8%/97.2%. More importantly, it is apparent that coupling efficiencies in Fig. 2 are robust against the critical dimension (CD) variations.

Simulated beam propagations through the three optimized ADCSWGs are displayed in Figs. 1(e)–1(g). As a reference, the simulated TE_0–TE_1 mode conversion in a conventional ADC of 200-nm coupling gap is also shown in Fig. 1(d). All geometrical parameters of this reference ADC are identical to those of the ADCSWG in Fig. 1(e) except for the coupling length and the sidewall corrugations. The comparison between Figs. 1(d) and 1(e) manifests that the evanescent field is dramatically enhanced in the gap region by introducing the subwavelength corrugations. Therefore, the coupling length is shortened from 17.0 μm to 5.6 μm.

As shown in Fig. 1(b), the minimal feature size of the ADCSWG occurs in its center, which is ~50 nm. However, for most

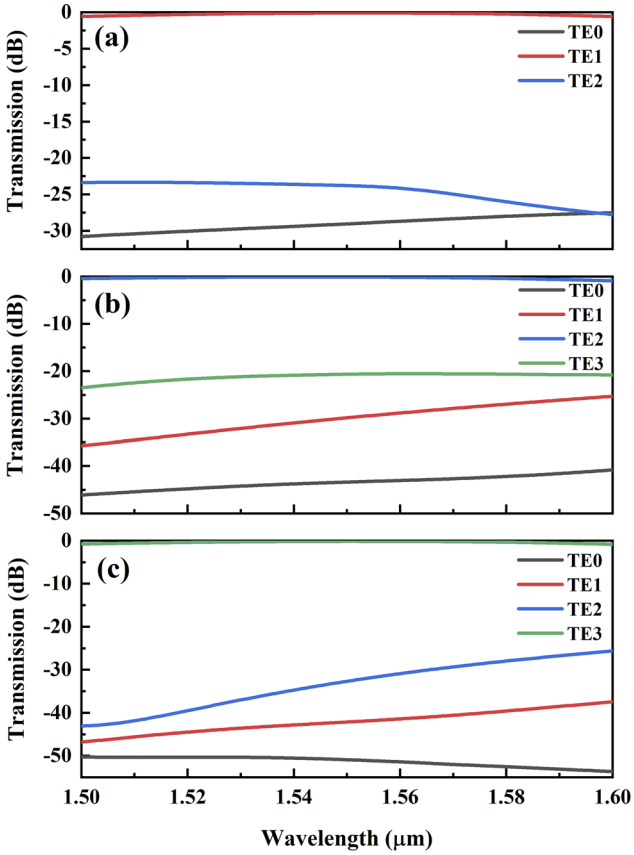

Fig. 3. Simulated transmission spectra of different modes in the three ADCSWGs: (a) TE_0–TE_1, (b) TE_0–TE_2, and (c) TE_0–TE_3.

of the region, the feature size is >100 nm. Compared with a conventional ADC with 50-nm uniform coupling gap, our device is more robust against fabrication errors [7,22] as will be presented in the following text.

Simulated transmission spectra of the three ADCSWGs over a wavelength range from 1.5 μm to 1.6 μm are shown in Figs. 3(a)–3(c). The three ADCSWGs offer low mode conversion losses and low mode cross talks within the wavelength range of interest. Specifically, the worst insertion losses and cross talks of the three devices are 0.5/0.8/0.7 dB and −23.4/−20.5/−25.8 dB, respectively.

The optimized device is fabricated on an SOI substrate with a 220-nm-thick top silicon layer and a 2-μm-thick buried oxide (BOX) layer. At first, waveguides are patterned by E-beam lithography (EBL) and inductively coupled plasma (ICP) dry-etching. After that, a 2-μm-thick SiO_2 layer is deposited as the top cladding by plasma-enhanced chemical vapor deposition (PECVD). A microscopy image of the fabricated device is shown in Fig. 4(a). It is a 4×1 mode multiplexer (with input ports I_0–I_3) which is connected directly to a 1×4 mode demultiplexer (with output ports O_0–O_3). Light is coupled into and out of the device through fiber grating couplers. Scanning electron microscopy (SEM) images of the three ADCSWGs are shown in Figs. 4(b)–4(d), where the sinusoidal corrugation is clearly distinguishable.

The device performance is characterized with an optical spectrum analyzer (Ando Electric/AQ6317C) and an amplified spontaneous emission light source (OPEAK/ASE171102)

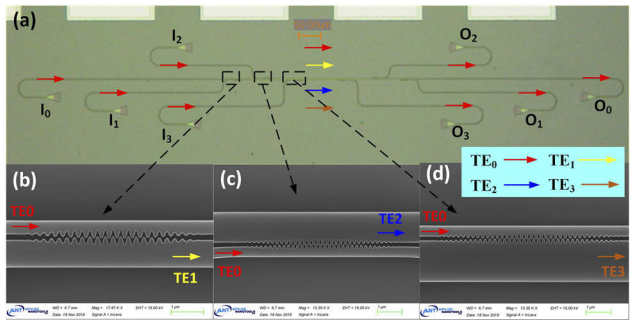

Fig. 4. (a) Microscopy image of the on-chip MDM link containing four mode channels. (b)–(d) SEM images of ADCSWGs to enable TE_0–$TE_{1/2/3}$ mode conversions.

whose bandwidth and center wavelength are 50 nm and 1555 nm, respectively. We switch the input port from I_0 to I_3, and then measure transmitted spectra at the four output ports. Results are displayed in Fig. 5 after normalizing coupling losses of the two grating couplers. The minimal and the maximum insertion losses over the 50-nm-wide wavelength span for TE_0–$TE_{0/1/2/3}$–TE_0 mode channels are 0.2/0.7/0.7/0.9 dB and 2.4/2.9/3.0/4.0 dB, respectively. The worst cross talk between the objective output port and the other three output ports are −18.0/−19.1/−16.0/−18.2 dB as the light is input from the $I_{0/1/2/3}$ ports. The measured transmission spectra in Fig. 5 are slightly worse than the simulation results in Fig. 3. The performance degradation can be attributed to fabrication imperfections such as deformed corrugation tooth, critical dimension variations, waveguide sidewall roughness, and write field stitching error of the EBL system [23].

To investigate the fabrication tolerance of the proposed structure, transmission spectra of the TE_0–TE_1 mode multiplexer under different CD variations are simulated in Figs. 6(a)–6(d). The simulation results indicate that the device performance is more sensitive to the coupling gap and the bus waveguide width.

Finally, our device is compared favorably with previously reported mode (de)multiplexers in Table 1 in terms of insertion loss, cross talk, minimal feature size, design difficulty, channel

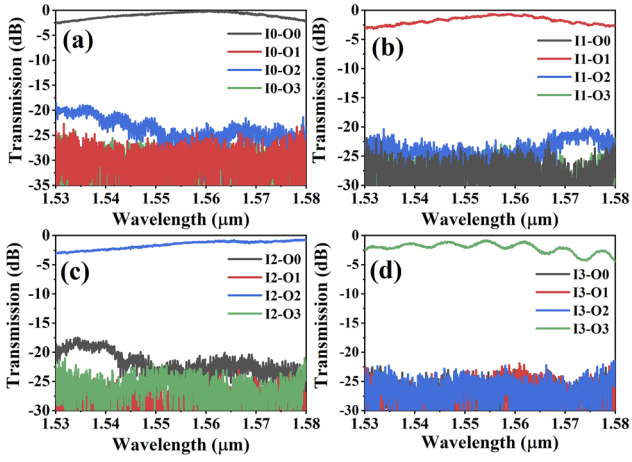

Fig. 5. Measured transmission spectra at the four output ports of the four-mode MDM link. Light is incident from the (a) I_0 port, (b) I_1 port, (c) I_2 port, and (d) I_3 port.

Table 1. Comparison of the Reported MDM[a]

Reference	Loss@1550 nm (dB)	Cross Talk (dB)	Feature Size (nm)	Bandwidth (nm)	Channel Count	Coupling Length of (TE0-TE1) (μm)	Design Difficulty
[16]	<1.7	> − 12.0	32	80	3	—	High
[17]	<1.2	−19.0 to −22.0	90	80	3	—	High
[11]	3.3–5.7	−9.7 to −31.5	NA	29	3	190	Low
[15]	<1.3	> − 23.0	160	100	4	150	Low
[9]	0.2–2.0	−11.0 to −20.0	200	100	8	15.5	Low
[24]	0.1–2.6	−15.4 to −26.4	100	50	10	18.5	Low
[25]	0.1–1.8	−15 to −25	120	90	10	15	Low
This work	**0.2–0.9**	**−16.0 to −19.1**	**50**	**50**	**4**	**5.6**	**Low**

[a]All devices are patterned by EBL.

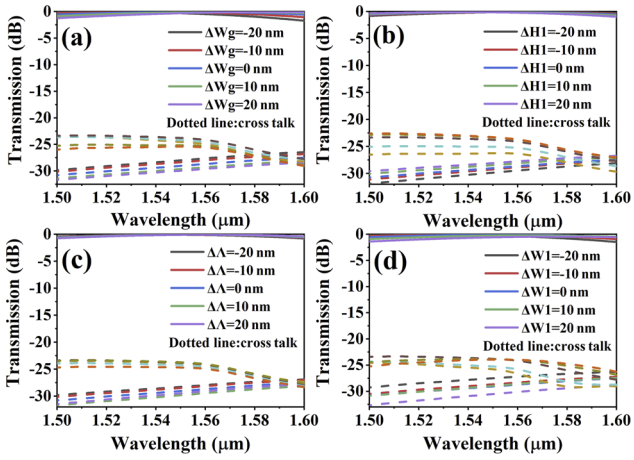

Fig. 6. Simulated transmission spectra of the TE_0–TE_1 mode multiplexer with fabrication errors in (a) the coupling gap W_g, (b) the maximum corrugation depth H_1, (c) the corrugation pitch Λ, and (d) the bus waveguide width W_1.

count, and footprint. Apparently, our device provides a satisfying trade-off between these performance metrics. In conclusion, we use the ADCSWG structure to realize an ultra-compact four-channel mode (de)multiplexer on silicon. The good synthetic performance of this device lend itself to a competitive candidate for MDM on silicon.

Funding. 800G optical transceiver chip and photonics engine of Zhejiang Lab (2020LC0AD02); Science and Technology Innovation 2025 Major Project of Ningbo (2020Z021); National Key Research and Development Program of China (2018YFB2200602).

Disclosures. The authors declare no conflicts of interest.

Data availability. Data underlying the results presented in this paper are not publicly available at this time but may be obtained from the authors upon reasonable request.

REFERENCES

1. A. Shacham, K. Bergman, and L. P. Carloni, IEEE Trans. Comput. **57**, 1246 (2008).
2. S. Perrin, *Heavy Reading* (2010).
3. K. Okamoto, IEEE J. Sel. Top. Quantum Electron. **20**, 248 (2014).
4. P. Dong, IEEE J. Sel. Top. Quantum Electron. **22**, 370 (2016).
5. T. Ye, Y. Fu, L. Qiao, and T. Chu, Opt. Express **22**, 31899 (2014).
6. D. J. Richardson, J. M. Fini, and L. E. Nelson, Nat. Photonics **7**, 354 (2013).
7. J. Wang, S. He, and D. Dai, Laser Photonics Rev. **8**, L18 (2014).
8. D. Dai, J. Wang, and Y. Shi, Opt. Lett. **38**, 1422 (2013).
9. D-X Dai and W. Jian, IEEE Photon. Soc. News **28**, IM2A.2 (2014).
10. Y. Kawaguchi and K. Tsutsumi, Electron. Lett. **38**, 1701 (2002).
11. W. Chen, P. Wang, T. Yang, G. Wang, T. Dai, Y. Zhang, L. Zhou, X. Jiang, and J. Yang, Opt. Lett. **41**, 2851 (2016).
12. M. Ye, Y. Yu, J. Zou, W. Yang, and X. Zhang, Opt. Lett. **39**, 758 (2014).
13. J. B. Driscoll, R. R. Grote, B. Souhan, J. I. Dadap, M. Lu, and R. M. Osgood, Opt. Lett. **38**, 1854 (2013).
14. C. Pan and B. A. Rahman, J. Lightwave Technol. **34**, 2288 (2016).
15. D. Guo and T. Chu, Opt. Express **25**, 9160 (2017).
16. L. F. Frellsen, Y. Ding, O. Sigmund, and L. H. Frandsen, Opt. Express **24**, 16866 (2016).
17. W. Chang, L. Lu, X. Ren, D. Li, Z. Pan, M. Cheng, D. Liu, and M. Zhang, Opt. Express **26**, 8162 (2018).
18. H. Xu and Y. Shi, Opt. Lett. **42**, 5202 (2017).
19. R. Cheng and L. Chrostowski, J. Lightwave Technol. **39**, 712 (2021).
20. L. Lu, D. Liu, F. Zhou, D. Li, M. Cheng, L. Deng, S. Fu, J. Xia, and M. Zhang, Opt. Lett. **41**, 5051 (2016).
21. R. Halir, P. J. Bock, P. Cheben, A. Ortega-Moñux, C. Alonso-Ramos, J. H. Schmid, J. Lapointe, D.-X. Xu, J. G. Wangüemert-Pérez, Í. Molina-Fernández, and Siegfried Janz, Laser Photonics Rev. **9**, 25 (2015).
22. Q. Jiang, G. Tao, and X. Chen, *Optoelectronic Devices and Integration VIII* (International Society for Optics and Photonics, 2019), , Vol. 11184, p. 1118409.
23. X. Zhao, Y. Wang, Q. Huang, and J. Xia, Opt. Express **25**, 2654 (2017).
24. Y. He, Y. Zhang, Q. Zhu, S. An, R. Cao, X. Guo, C. Qiu, and Y. Su, J. Lightwave Technol. **36**, 5746 (2018).
25. D. Dai, C. Li, S. Wang, H. Wu, Y. Shi, Z. Wu, S. Gao, T. Dai, H. Yu, and H.-K. Tsang, Laser Photonics Rev. **12**, 1700109 (2018).